Journal of Power Sources 212 (2012) 192–204

Contents lists available at SciVerse ScienceDirect

Journal of Power Sources

journal homepage: www.elsevier.com/locate/jpowsour

Hybrid fuel cell powertrain for a powered wheelchair driven by rim motors

Yee-Pien Yang*, Ruei-Ming Guan, Yen-Ming Huang

Department of Mechanical Engineering, National Taiwan University, 1 Roosevelt Road, Sec. 4, Taipei 106, Taiwan, ROC

ARTICLE INFO

Article history:
Received 26 February 2012
Accepted 5 April 2012
Available online 17 April 2012

Keywords:
Energy management
Hybrid fuel cell powertrain
Powered wheelchair
Rim motor

ABSTRACT

This paper proposes a hybrid fuel cell powertrain for a powered wheelchair driven by rim motors. Since this innovative wheelchair claims to be light, foldable, and fuel efficient, it would be more promising to have a fuel cell powertrain that is self-charged, extractable, and small in size and weight. The proposed hybrid fuel cell powertrain combines a fuel cell and two secondary battery packs with enough power but minimal in size and weight for the wheelchair. The fuel cell unit is responsible only for charging one of the battery packs, while the other battery by turns supplies power to load. This energy management strategy improves the power fluctuation of the fuel cell as well as reduces the charge frequency of the secondary battery. The effectiveness of the proposed powertrain is evaluated and compared with a traditional hybrid fuel cell powertrain with simulations and experiments, which prove that the output power of the fuel cell is nearly constant and the number of charges is reduced by 98%.

1. Introduction

Fast development of modern medical technology has made welfare issues of the aging population and health care important in the government's social and political policies. Various assistive mobility devices, such as wheelchairs and shopriders, have become indispensable for helping the aged and the disabled extend their range of activity and have better quality of life. The powered wheelchair is especially essential for those who are able to travel by themselves without additional assistance.

Most commercial powered wheelchairs have secondary batteries, such as lead acid, nickel metal-hydride, or lithium-ion batteries, installed as a power source. For increased driving range and a higher discharge rate, a larger secondary battery pack in size and weight is usually necessary. Powered wheelchairs therefore become bulky and heavy. Furthermore, the location and time spent charging the battery on the wheelchair may result in a bad experience for the user when the wheelchair runs out of power during a journey. Therefore, a powered wheelchair may require a powertrain of energy storage units with two desired features. First, the power density must be as high as possible for the wheelchair to operate well with various accelerating and cruising driving patterns. Second, the energy density should be so high that the wheelchair has enough capacity for a long driving range but with less weight.

Secondary batteries have good power density with a high discharge rate, while a fuel cell is a renewable energy source of high energy density. Thus, a hybrid fuel cell powertrain combining fuel cells and secondary batteries is suggested for a powered wheelchair to improve its fuel economy and cycle life [1,2]. In addition, a secondary battery is able to compensate a fuel cell for its weak performance in output power response and fluctuation [3,4]. Moreover, the plug-in charge from city electricity may become unnecessary, because the fuel cell unit with its own hydrogen canister in the hybrid powertrain is responsible for charging the battery and/or supplying power to load. Since it is not necessary for the hybrid fuel cell powertrain to take a fast charge from the fuel cell unit to the secondary battery, a moderate charge rate must prolong the lifetimes of the fuel cell and battery. A few studies also included ultra-capacitors in the hybrid fuel cell powertrain for a huge power discharge during a very short period [5,6].

Traditional hybrid fuel cell powertrains are classified into two categories: series and parallel, which follow the similar classification for hybrid electric vehicles [7–9]. A series-hybrid fuel cell powertrain basically consists of a low-power fuel cell, a dc/dc converter, and a secondary battery of higher capacity, while a parallel-hybrid fuel cell powertrain is usually composed of a high-power fuel cell stack, a secondary battery pack of lower capacity, and a bidirectional dc/dc converter. The series- and parallel-hybrid powertrain needs an energy management unit to improve the fuel economy, efficiency, and performance of the fuel cell, subject to the load variation and the state of charge (SOC) of the battery. The power split strategy from the fuel cell system to secondary batteries or ultra-capacitors has become the main concern in many

* Corresponding author. Tel.: +886 2 3366 2682; fax: +886 2 2363 1755.
E-mail address: ypyang@ntu.edu.tw (Y.-P. Yang).

0378-7753/$ – see front matter © 2012 Elsevier B.V. All rights reserved.
doi:10.1016/j.jpowsour.2012.04.012

publications. Most studies referred to the parallel type of hybrid fuel cell powertrain, either in simulations [10–17] or in experiments and implementations [18–25], but fewer referred to the serial type of hybrid fuel cell powertrain [26–30].

Two significant problems occurred in previous research on the energy management strategy of hybrid fuel cell powertrains [12,31–33]. One was the frequent charge from the fuel cell to the battery when the load varied due to changeable driving modes. A battery subject to frequent charging would age fast and its performance would deteriorate [34]. The other serious problem was the fluctuation of the output power of the fuel cell, which might be closely related to age and decay. Unfortunately, these problems were usually solved by increasing the power of the fuel cells and secondary batteries, thereby increasing their size, weight, and cost.

In this paper, a hybrid fuel cell powertrain and an energy management strategy are proposed to improve the drawbacks of traditional hybrid fuel cell powertrains and to increase the energy utilization efficiency. A platform of a powered wheelchair for investigating the performance of the proposed powertrain is introduced in Section 2, where the energy storage components are selected according to the driving specifications. Section 3 introduces the energy management strategy of the proposed powertrain. The output performance of the proposed powertrain is evaluated in Section 4 through simulations and experiments, and Section 5 concludes the research.

2. Material and methods

2.1. Platform

The proposed hybrid fuel cell powertrain is to be implemented on a novel powered wheelchair driven by rim motors, as shown in Fig. 1. The rotor of the rim motor is a conventional push rim, in which a series of magnets with alternate N and S poles are plugged. Two sectors of the arc stator are designed facing the inner side of the rim. The rim motor described herein exerts force around the wheel rim, resembling the force given by the user to generate enlarged torque with a large rim radius. The large wheel also provides better mobility over rough surfaces.

The application of rim motors on the powered wheelchair is very promising. The stator, rim rotor, and wheel can be assembled as one component to replace any commercial wheel of the same size. The stator need not necessarily be a circle but an arc shaped in any angle. The empty space between the stator allows a driver to push on the rim as easily as driving a manually driven wheelchair when the power is off. Two driving wheels with rim motors are then installed on each side of the wheelchair to form a foldable structure. This configuration enables a larger force arm that multiplies the force exerted along the rim to produce a larger torque than the conventional hub-in motor with a smaller radius. An optimal design procedure for a rim motor has made the electric-powered wheelchair foldable, light, fuel efficient, and easy to operate [35]. The specifications are illustrated in Table 1.

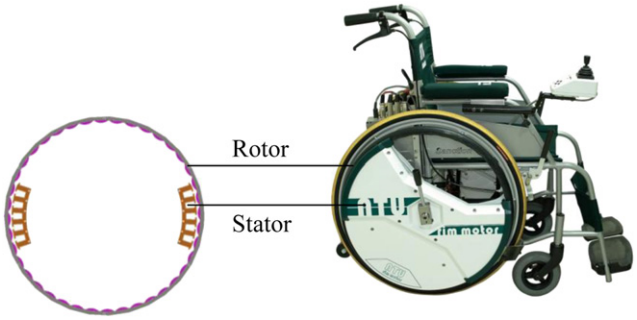

Fig. 1. Prototype of a powered wheelchair driven by rim motors.

Table 1
Specifications of wheelchair.

Gross weight	30 kg	Wheel radius	30 cm
Loading	80 kg	Energy storage	16 kg
Rim motor	24 V, 29 Nm, 90 rpm, 250 W max. (each)		
Acceleration	0.51 m s^{-2}, 9.4 km h^{-1} on level surface		
Max. speed	0.49 m s^{-2}, 4.6 km h^{-1} on slope surface (8:1)		

2.2. Traditional hybrid fuel cell powertrains

There are many combinations of fuel cell with auxiliary energy storage systems for a powered wheelchair, such as a fuel cell with secondary batteries and/or ultra-capacitors. The most commonly used hybrid fuel cell powertrain is a combination of a fuel cell and secondary batteries, connected in series or parallel. Before the proposed powertrain is introduced, the features of traditional hybrid fuel cell powertrains are reviewed as follows.

The series-hybrid fuel cell powertrain basically includes a low-power fuel cell, a dc/dc converter, and a secondary battery of high capacity, as shown in Fig. 2. This configuration is also called an energy-hybrid powertrain, for the main benefit is to extend the driving range. Both the fuel cell and battery supply power to the load. At a light load, the fuel cell is able to offer all the power requested by the load, while charging the remnant power to the battery. At a heavy load, the secondary battery pack supplies the most power requested by the load, while the fuel cell assists the rest of the power to the load.

The parallel-hybrid fuel cell powertrain is usually composed of a high-power fuel cell stack, a secondary battery pack of low capacity, and a bidirectional dc/dc converter, as shown in Fig. 3. This configuration is also called a power-hybrid powertrain, where the fuel cell provides the primary power demanded by the load. The secondary battery discharges power only when the wheelchair is accelerating or climbing a slope while the fuel cell is not able to provide enough power. The battery is usually charged by the fuel cell at a light load or by power from regenerative braking.

A common problem for the fuel cell either in the series- or parallel-hybrid powertrain is its frequent charging to the secondary battery due to load variation, which must cause fuel starvation, membrane flooding or drying, and the imbalanced pressure difference between the two sides of the cell membrane [5,27,36]. These damage the fuel cell stack and shorten its life.

2.3. Proposed hybrid fuel cell powertrain

The proposed hybrid fuel cell powertrain for the powered wheelchair includes a fuel cell, a dc/dc converter, and two secondary battery packs, as shown in Fig. 4. Since the ultra-capacitor has a much smaller energy density than the fuel cell and secondary battery, the ultra-capacitor is not considered in this research. The principal strategy of this proposed hybrid fuel cell powertrain is to assign independent responsibilities to the fuel cell and battery packs. The fuel cell is assigned only for charging one of the battery packs, while the other battery is responsible only for discharging power to the load. Therefore, the fuel cell is able to charge the battery at a stable and constant power level so that the internal resistance of the battery varies insignificantly. When one battery is discharging power to the load, the other one is charged by the fuel cell or idled. And the battery is charged only when its SOC is

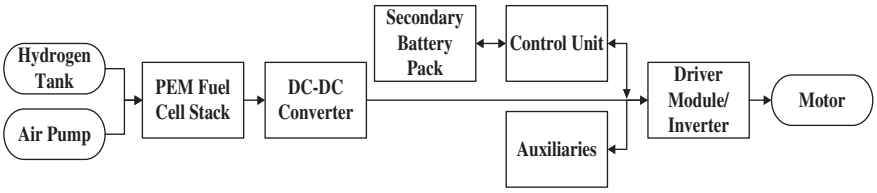

Fig. 2. Series-hybrid fuel cell powertrain.

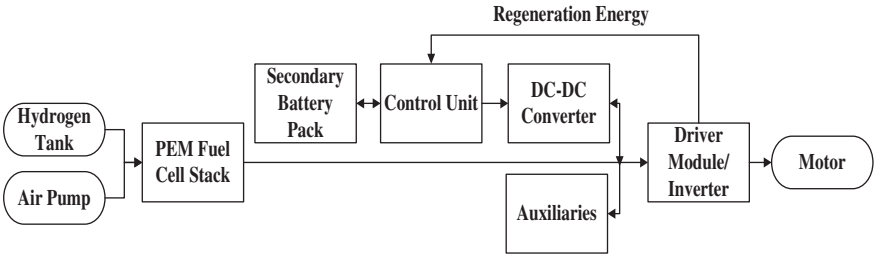

Fig. 3. Parallel-hybrid fuel cell powertrain.

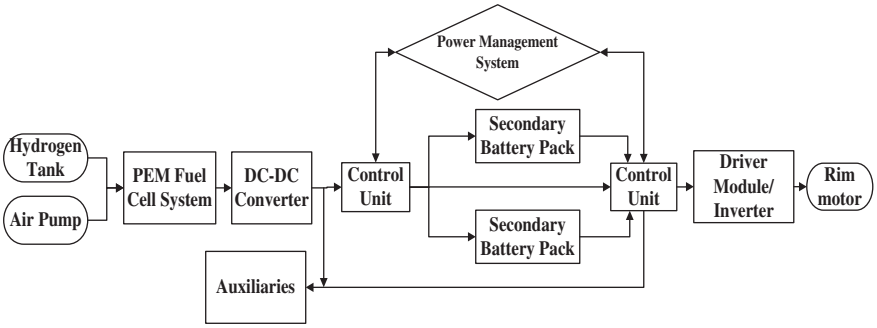

Fig. 4. Proposed hybrid fuel cell powertrain.

lower than a specific value. The following sections will investigate the utilization efficiency and power management strategy of the proposed powertrain.

2.4. Selection of energy storage components

The load requirement for the powered wheelchair driven by rim motors must be analyzed before a suitable set of fuel cell and batteries is selected. According to the input and output power curves versus the speed of rim motor of the wheelchair in Fig. 5, an investigation of various periodic driving patterns was performed. A peak power of 678 W was provided for the wheelchair to accelerate or climb a slope, and consecutively 305 W was provided for the wheelchair to cruise at a rated motor speed of 45 rpm. Table 2 describes those driving patterns and their corresponding average power demands. The minimum power for the proposed powertrain must be higher than 393 W.

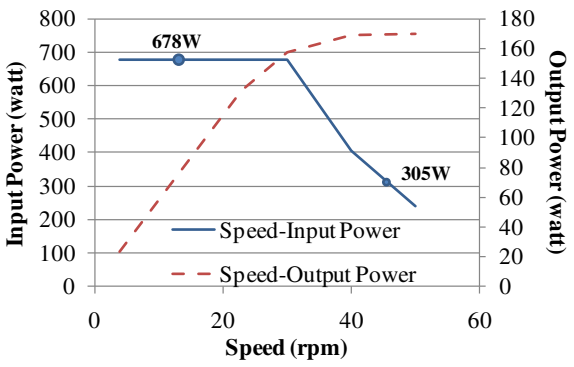

Fig. 5. Power vs. speed curves of the rim motor of wheelchair.

In addition to the load power analysis, additional issues are taken into consideration for choosing a complete fuel cell system, including a fuel cell stack, hydrogen tank, and the BOP. A commercial powered wheelchair is usually heavy and bulky; therefore, installation of a powertrain of unacceptable volume and weight is not recommended. Although a larger fuel cell could operate with higher efficiency, it would be ineffective in cost, weight, and volume, and its power and energy density may not be satisfactory. Especially, a large fuel cell stack is usually equipped with a large BOP, which may consume significant power from the power generated by the fuel cell itself. Among various types of fuel cells, the proton exchange membrane fuel cell (PEMFC) is a suitable option for the powered wheelchair driven by rim motors, because of the PEMFC's low operating temperature, high-power density, long durability, and low corrosiveness.

An air-breathing PEMFC of HEStack500 of HEPHAS is therefore selected, whose specifications are described in Table 3. The cathode side has an air inlet with cooling fans, and therefore the stack size is

Table 2
Driving pattern and average power.

Driving pattern	Time for peak power 678 W	Time for cruise power 305 W	Average power
A	5 s	20 s	393 W
B	5 s	60 s	334 W
C	5 s	120 s	320 W
D	5 s	240 s	313 W
E	5 s	480 s	308 W

Table 3
Specifications of HEStack500 of HEPHAS.

Nominal power	500 W(net)
Nominal voltage	19.2 V
Nominal current	26 A
Operation region	15–29 V
No. of cells	32
Reactive area	60 cm^2
Efficiency	≧50%
Fuel purity	≧99.95%
Fuel pressure	0.5–0.6 bar
Humidification	Self-humidify
Oxidant/coolant inlet	Air-breathing
Inlet pressure	Ambient pressure
Weight	2.8 kg
Volume (length × width × height)	176 × 173 × 115 mm
Surrounding temperature	−5 to 40 °C
Surrounding humidity (RH)	20–95%

greatly reduced. The net power of HEStack500 is estimated after the power consumed by the BOP is deducted, and it is able to recover a secondary battery pack of 400 W. The efficiency of this fuel cell is therefore estimated to be 47% at its working power of 400 W.

On the other hand, the secondary battery of the proposed powertrain should have enough capacity to drive the rim motors of the wheelchair during various driving patterns. From a list of commercially available secondary batteries in Table 4, lithium-ion batteries, having the highest energy and power density, are our first choices subject to space limitations. Since the safety and life cycle are the primary concerns for the secondary battery of powered wheelchairs, the lithium iron phosphate ($LiFePO_4$) battery becomes the final choice among the most commonly used lithium-ion batteries, as shown in Table 5.

The selected $LiFePO_4$ battery pack consists of 8 serially connected cells, each with 3.2 V and 10 A h capacity [37]. Since each cell has large capacity, the number of cells of the battery pack can be reasonably reduced, and the probability of cell failure can also be reduced. This battery pack can discharge in a rate of 1.3–3 C, while the suggested charging rate is 1.5 C. It would be better to operate the battery between the SOC range of 20–80%. In a practical way, the SOC of the $LiFePO_4$ battery pack is usually measured by a combination of Coulomb counting and open-circuit voltage (OCV).

Table 4
Comparison of commercially available secondary batteries.

Types	Energy density (W h kg^{-1})	Power density (W kg^{-1})	Efficiency (%)	Life (cycles)
Lead acid	30–45	200–300	>80	400–1000
Ni–Cd	40–60	150–350	75	600–1200
Ni–Zn	60–65	150–300	65	300
Ni-MH	60–70	150–300	70	600–1200
Zn–air	230	105	60	NA
Li-polymer	155	315	>95	600
Li-ion	90–130	250–450	>95	800–1200+

Table 5
Comparison of lithium-ion battery series.

Positive material	$LiMn_2O_4$	$LiCoO_2$	$LiNi_{1/3}Co_{1/3}Mn_{1/3}O_2$	$LiFePO_4$
Cell voltage (V)	3.7	3.6–3.7	3.6–3.7	3.4
Energy density (mA h g^{-1})	110	160	190	160
Life (cycle)	>500	>500	>500	>1000
Safety	Good	Acceptable	Acceptable	Best
Cost	Low	High	High	Low
Characteristic	Power	Energy	Power/energy	Power

3. Theory and calculation

3.1. Energy management strategy

The principal objective of a power management strategy is to maximize the energy utilization efficiency of the secondary battery. Its charge efficiency is defined as

$$\eta_c = V_h/V_c \quad (1)$$

where V_c is the battery's charging voltage, and V_h is the thermodynamic voltage of $LiFePO_4$ battery chemical reaction which is calculated as 3.7 V per battery cell. In contrast, the discharge efficiency of the secondary battery is defined as

$$\eta_d = V_d/V_h \quad (2)$$

where V_d denotes the battery's discharge voltage. When this discharge efficiency is used for a PEMFC, the thermodynamic voltage V_h is usually calculated as 1.48 V according to the higher heating value that describes the change in enthalpy of formation during the basic reaction for the hydrogen/oxygen fuel cell [7]. Both the charge and discharge efficiencies are regarded as energy utilization efficiencies as functions of operating temperature. In general, the energy utilization efficiency decreases as the cell temperature rises due to high-power dissipation, thereby damaging cell performance and safety.

According to the relationship between the energy utilization efficiency and the SOC of a secondary battery, as shown in Fig. 6 [38], one of the secondary battery packs of the powertrain should be discharged at a high SOC to load, while the other should be

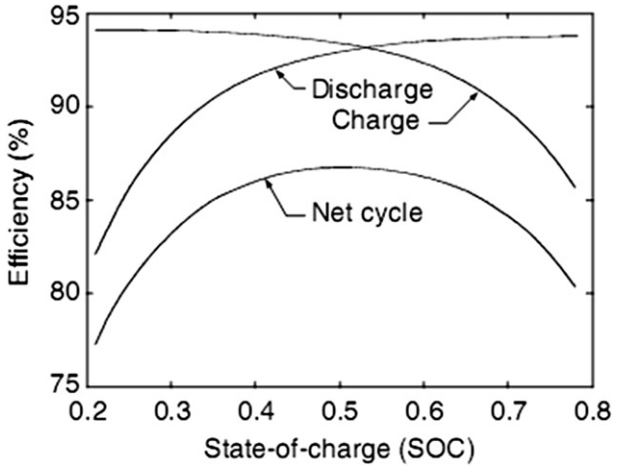

Fig. 6. Charge and discharge efficiencies versus SOC of a secondary battery [38].

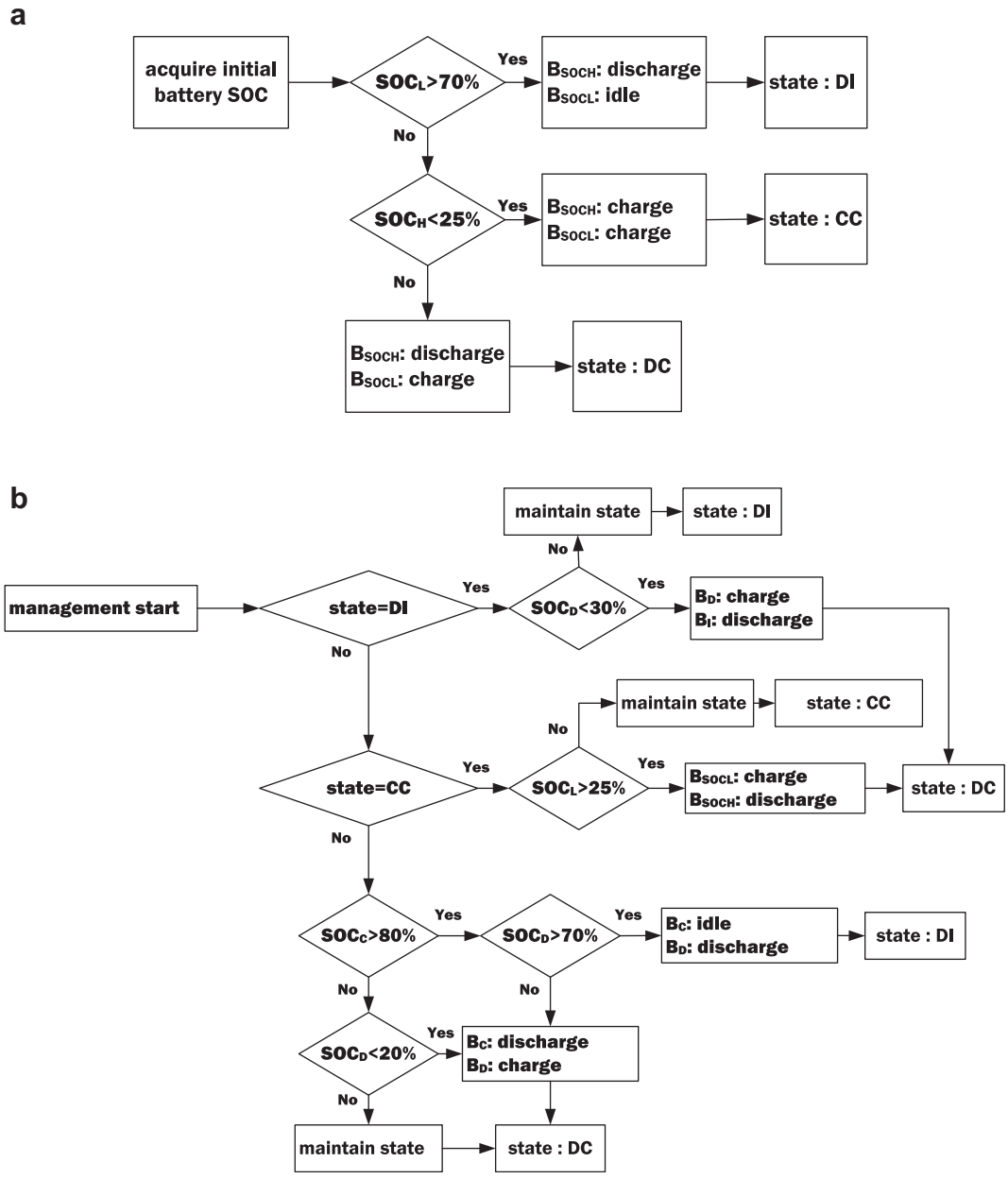

Fig. 7. Logic flow of energy management of the proposed powertrain at (a) initialization and (b) standard operation.

charged at a low SOC by the fuel cell. If both battery packs are full of charge, the fuel cell can rest to save fuel. In the worst case when both battery packs fail, the fuel cell must directly supply power to the rim motors of wheelchair. The average SOC of battery pack should be maintained as high above 50% as possible to reduce storage degradation. However, the reduction of the frequency of charge and discharge is another significant concern in the following logic flow chart of the energy management system of the proposed hybrid fuel cell powertrain, as shown in Fig. 7. The management logic first evaluates the SOC values of both batteries, where the battery with higher SOC is denoted by B_{SOCH} while the battery with lower SOC is denoted by B_{SOCL}. Any battery which is charged by fuel cell is denoted by B_C, the one which is discharging power to the load is denoted by B_D, while the one in the idle state is denoted by B_I. The symbol SOC_L means the SOC of the battery of lower SOC, and SOC_H means the SOC of the battery of higher SOC. Similarly, SOC_C denotes the SOC of the battery that is charged by fuel cell, and SOC_D is the SOC of the battery that is discharging power to the load.

3.2. Operation scenarios

Normally, one of the two batteries is responsible for driving the wheelchair, while the other is charged by the fuel cell or rests in the idle state. There are many possible scenarios during the operation of the powered wheelchair. Scenarios in initialization and standard operation are illustrated as follows.

3.2.1. Initialization

When the powertrain is on, the OCV of each battery is measured and its corresponding SOC is estimated according to the OCV versus SOC curve, as shown in Fig. 8. The initialization flow chart is illustrated in Fig. 7(a).

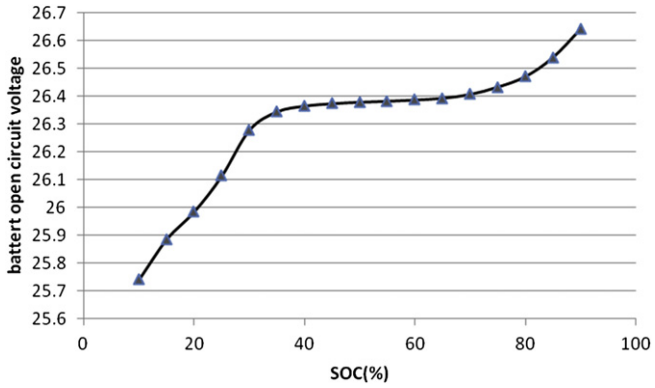

Fig. 8. Open-circuit voltage versus SOC of the secondary battery.

(A.1) As the SOCs of both batteries are higher than 70%, the battery of higher SOC starts discharging power to the load, while the other battery stays in the idle state. This state of operation is denoted by State DI.
(A.2) As the SOCs of both batteries are lower than 25%, the fuel cell starts to charge both batteries without supplying power to the load. This state of operation is denoted by State CC.
(A.3) Otherwise, the battery of higher SOC starts to supply power to the load, while the other is charged by the fuel cell. This state of operation is denoted by State DC.

3.2.2. Standard operation

Case 1: State DI is identified.
(B.1) If the SOC of the battery in the discharge state is still higher than 30%, then the current State DI is maintained.
(B.2) Otherwise, the battery that was in the idle state starts to supply power to the load, while the other that was in the discharge state is shifted to be charged by the fuel cell. The powertrain comes to State DC.

Case 2: State CC is identified.
(B.3) If the SOCs of both batteries are detected higher than 25%, the battery of higher SOC starts to supply power to the load, while the other maintains the charge state. The powertrain comes to State DC.
(B.4) Otherwise, State CC is maintained.

Case 3: State DC is identified.
(B.5) If the SOC of the other battery that is charged by the fuel cell is found higher than 80% and the SOC of the battery that is supplying power to the load is higher than 70%, the former must be shifted to the idle state because the charging efficiency will be low for the battery with a SOC higher than 80%. The battery that was supplying power to the load maintains its current discharge state. The powertrain therefore becomes State DI.
(B.6) But if the SOC of the battery that is supplying power to the load is lower than 70%, this battery will be shifted to the charge state, while the other battery that has been charged over 80% is shifted to the discharge state. The powertrain is still in State DC but two batteries are switched to different tasks.
(B.7) If the SOC of the battery that is charged by the fuel cell is lower than 80% (that must be higher than 25% from initial state), and the SOC of the other battery that is supplying power to the load is lower than 20%, the battery tasks must be switched each other. The powertrain is still in State DC.
(B.8) If the above three conditions are not identified, the current powertrain State DC is maintained.

However, abnormal situations may happen as follows:

(1) If the two batteries are out of power, the fuel cell itself will provide power to the wheelchair.
(2) If the fuel cell is out of power or fuel is depleted, the two batteries will provide power to the wheelchair together.
(3) If the fuel cell and the batteries are all out of power, the wheelchair has to be driven manually.

4. Results and discussion

4.1. Energy component models

Before the proposed hybrid fuel cell powertrain and its energy management strategy to the powered wheelchair driven by rim motors was implemented, simulations were performed by using the MATLAB Simulink and SimPowerSystems Toolbox, which included various power elements of secondary battery and fuel cell models [39].

The hydrogen and oxidant utilizing efficiency are calculated [7,40], respectively, as

$$U_{f_{H_2}} = \frac{60,000RT\,i_{fc}}{zFP_fV_fx} \tag{3}$$

and

$$U_{f_{O_2}} = \frac{60,000RT\,i_{fc}}{2zFP_aV_ay} \tag{4}$$

where R is the ideal gas constant, T is the absolute operating temperature, i_{fc} is the fuel cell current, z is the number of reacting electron in chemical reaction formula, F is Faraday constant; P_f, P_a, V_f and V_a are, respectively, the fuel and air inlet pressures and flow rates; while x and y denote, respectively, the percentage of the hydrogen purity of fuel and the oxygen purity of air. The hydrogen and oxygen utilizing efficiency are used to calculate the hydrogen partial pressure P_{H_2}, the oxygen partial pressure P_{O_2}, and the vapor partial pressureP_{H_2O} as

$$P_{H_2} = \left(1 - U_{f_{H_2}}\right)xP_f \tag{5}$$

$$P_{O_2} = \left(1 - U_{f_{O_2}}\right)yP_a \tag{6}$$

$$P_{H_2O} = \left(w + 0.02U_{f_{O_2}}\right)P_a \tag{7}$$

where w is the air humidity.

According to Nernst equation, the Nernst voltage can be expressed as

$$E_n = 1.229 + (T - 298)\frac{-44.43}{zF} + \frac{RT}{zF}\ln\left(P_{H_2}P_{O_2}^{1/2}\right). \tag{8}$$

The fuel cell voltage E_{fc} is expressed as

$$E_{fc} = K_cE_n - NA\frac{1}{sT_d/3 + 1}\ln\left(\frac{i_{fc}}{i_0}\right) - R_{fc}i_{fc} \tag{9}$$

where K_c is the standard operating voltage constant, N is the number of cells in the fuel cell stack, A is Tafel coefficient, i_0 is the exchange current density, and R_{fc} is the internal resistance of the fuel cell. The first order term $1/(sT_d/3+1)$ models the activation

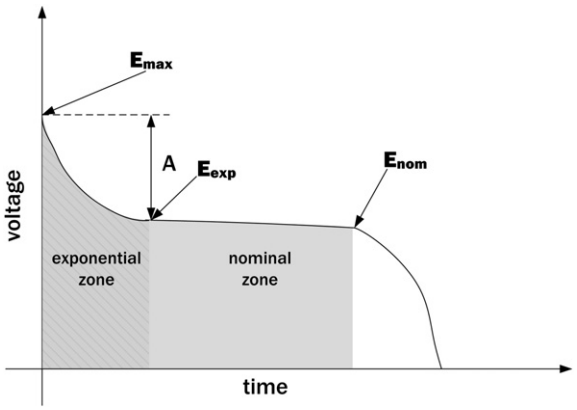

Fig. 9. General discharge voltage versus time curve for a secondary battery.

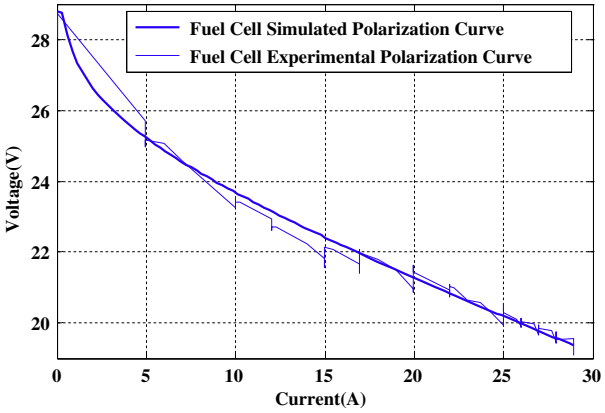

Fig. 10. PEMFC performance of simulation and experiment.

polarization of the fuel cell as an equivalent parallel RC circuit, where $T_d/3$ is the time constant.

The open-circuit voltage E of the secondary battery in the simulation is modeled as [41]

$$E = E_0 - K\frac{Q}{Q - \int_0^t i\mathrm{d}\tau} + A\exp\left(-\frac{3}{Q_{\mathrm{exp}}}\int_0^t i\mathrm{d}\tau\right) \quad (10)$$

$$E_0 = K + R_{\mathrm{b}}i - E_{\mathrm{exp}} \quad (11)$$

$$K = \left[(E_{\mathrm{max}} - E_{\mathrm{nom}}) + (E_{\mathrm{max}} - E_{\mathrm{exp}})\left[\exp\left(-\frac{3Q_{\mathrm{nom}}}{Q_{\mathrm{exp}}}\right) - 1\right]\right] \times \left(\frac{Q}{Q_{\mathrm{nom}}} - 1\right) \quad (12)$$

where E_0 is the ideal battery voltage, K is the polarization voltage coefficient, R_{b} is the internal resistance of the secondary battery, and Q is the total battery capacity. According to Fig. 9, E_{max} and E_{exp} are, respectively, the maximum and minimum battery voltages of the exponential zone; Q_{exp} and Q_{nom} are, respectively, the battery capacities of the exponential and nominal zones; while E_{nom} is the battery voltage at the end of nominal zone. Therefore, the loading voltage of the secondary voltage E_{b} is calculated as

$$E_{\mathrm{b}} = E - R_{\mathrm{b}}i. \quad (13)$$

The effectiveness of the fuel cell model was investigated by comparing its polarization curves from simulation and experiment. Fig. 10 shows the simulated polarization curve for HEStack500, which is nearly the same as the experimental one, especially as the current was higher than 17 A. Simulation parameters were assigned close to the operation conditions for experiments, such as the operating temperature of the fuel cell at 55 °C, the nominal air flow at 20 lpm, the nominal supply pressures for fuel and air, respectively, at 1.4 and 1.0 bar. Similarly, the discharge curves of the $LiFePO_4$ battery in the simulation and experiment were also closely consistent, as shown in Fig. 11. Since this paper focuses only on the energy management of the hybrid powertrain, details in thermal effect and water management and their influence on system dynamics were not investigated.

Other components of the powertrain were given as follows. The Ovonics solid hydrogen storage canister had a capacity of 240 L. The hydrogen consumption rate in the HEStack500 fuel cell was

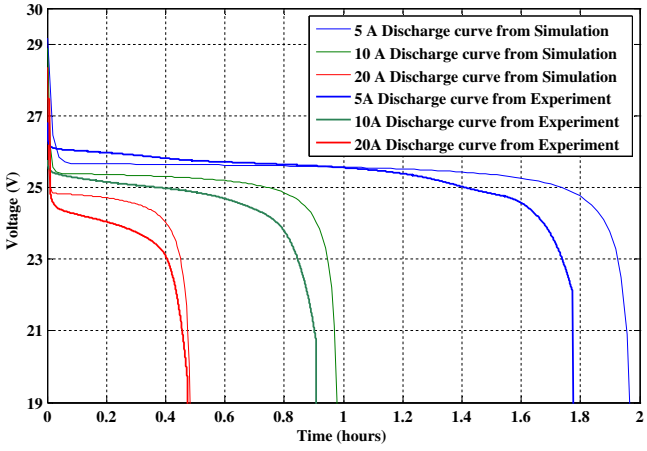

Fig. 11. $LiFePO_4$ battery pack performance of simulation and experiment.

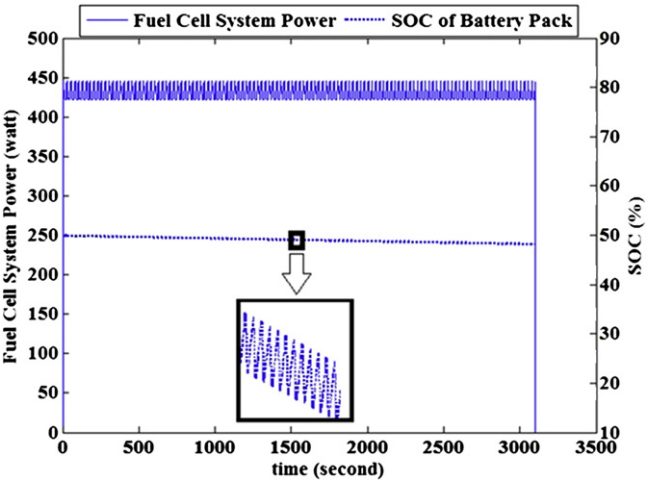

Fig. 12. Performance of the series-hybrid fuel cell powertrain.

approximated by a 6th power polynomial as a function of fuel cell power. In addition, the load was simulated by two resistors to absorb the power from the $LiFePO_4$ battery packs. To simulate a real

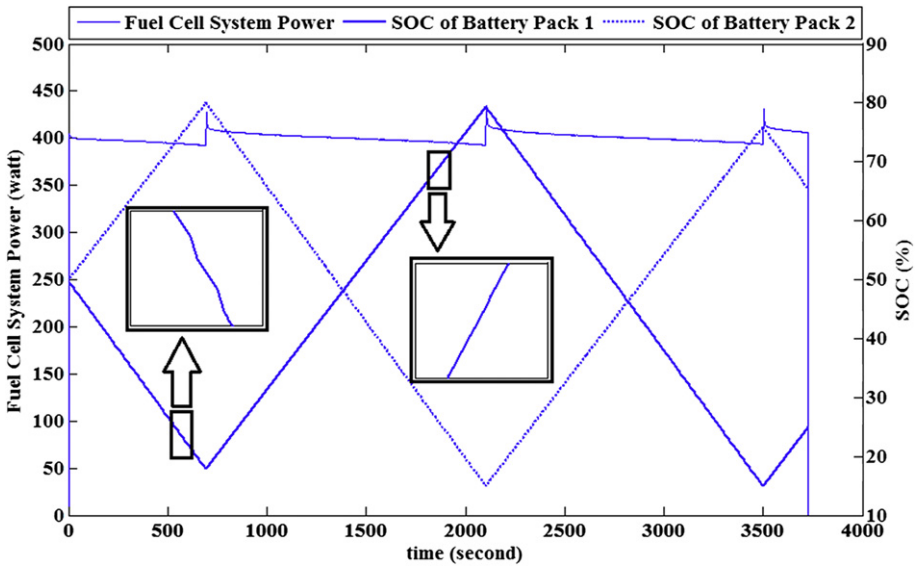

Fig. 13. Performance of the proposed hybrid fuel cell powertrain.

motor drive circuit, a controllable source in the load block was assigned to keep the load voltage at 24 V.

4.2. Comparison between traditional and proposed powertrains

Among the traditional hybrid fuel cell powertrains, the size of the hybrid powertrain in series is usually smaller than that in parallel because of the BOP of the series-hybrid powertrain is smaller. Therefore, the proposed hybrid fuel cell powertrain was simulated and compared with the series-hybrid fuel cell powertrain of the same components. The initial SOC of $LiFePO_4$ battery pack of 10 A h was set at 50%. The wheelchair's periodic driving pattern was assigned to accelerate for 5 s to consume a higher average power of 678 W and then to cruise for 20 s at a lower power consumption of 305 W.

The energy management system operated for the proposed hybrid fuel cell powertrain according to the strategy introduced in Section 3, where the fuel cell was responsible only for charging the secondary battery. In contrast, the fuel cell of the series-hybrid powertrain always supplied power to load, and charged the battery with its remnant power if its current SOC was less than 80%. The output power of the fuel cell and the SOC of battery packs in the series- and proposed hybrid fuel cell powertrain are shown in Figs. 12 and 13, respectively. Table 6 compares the performance between these two hybrid fuel cell powertrains.

It is not surprising that the proposed hybrid fuel cell powertrain charged only twice over 4000 s, which was much less than 135 times of charge with the series-hybrid fuel cell powertrain. The number of charges was greatly reduced by 98.5%. The operation time of the proposed hybrid powertrain was also longer than the series-hybrid powertrain. Furthermore, the variation of the output power of the fuel cell and the battery in the proposed hybrid powertrain was much smaller than that in the series-hybrid powertrain. These results demonstrate that using hydrogen is efficient

Table 6
Simulation results of series- and proposed hybrid fuel cell powertrain.

Powertrain structure	Series	Proposed
Average load power	394.8 W	
Charging moment of SOC	Uncertain	SOC < 20%
Average fuel cell power (W)	427.6	397.5
Operation time of fuel cell (s)	3161	3788
Initial SOC (%)	50	50
Final SOC (%)	48	44.9
Average operation time (s)	3388	3854
No. of charges	135	2

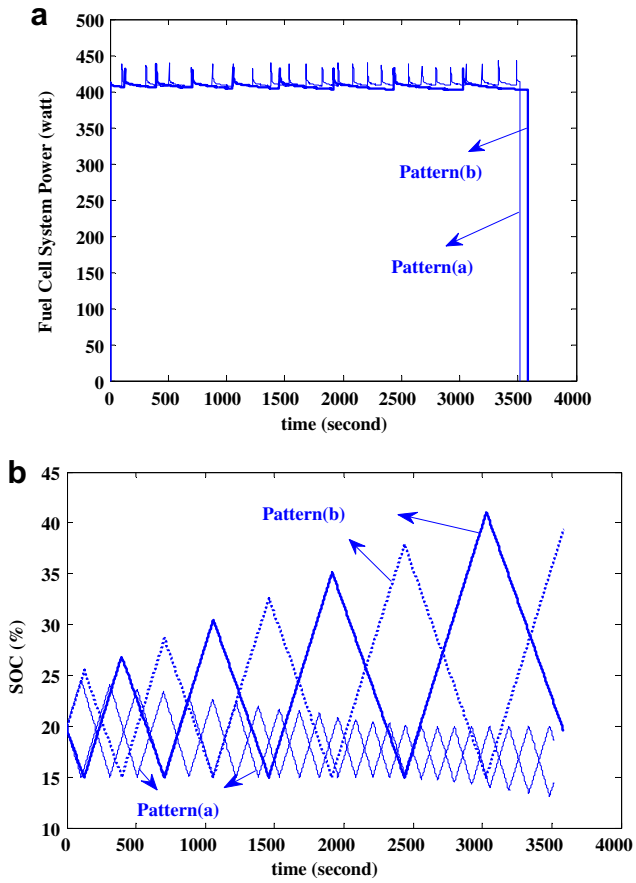

Fig. 14. Variation of (a) the output power of fuel cell and (b) the SOC of both batteries for different driving patterns by the proposed hybrid powertrain.

Table 7
Simulation results of the proposed hybrid fuel cell powertrain under different driving patterns.

Driving pattern	(a)	(b)
Acceleration/cruise period (s)	5/20	5/60
Average load power (W)	395	334
Average fuel cell power (W)	412	408.4
Fuel cell operation time (s)	3485	3564
Initial SOC (%)	20,20	20,20
Final SOC (%)	18.7, 14.5	19.5, 39.4
Average operation time (s)	3494	3564
No. of charges	12	5

for the proposed hybrid powertrain, and the size and cost of the fuel cell system can be greatly reduced.

4.3. Performance under different driving cycles

In the previous section, a short-cruise driving pattern (a) was simulated, which was a strict driving mode of accelerating the wheelchair with an average power of 678 W for 5 s, and cruising with 305 W for 20 s. In real life, a long-cruise driving pattern (b) may happen often and was simulated by periodically accelerating the wheelchair for 5 s and cruising for 60 s. The initial SOC of the $LiFePO_4$ battery was set at 20% for both driving patterns under the operation of the proposed hybrid powertrain. According to the energy management strategy, the fuel cell was responsible only for charging one of the two battery banks or rested when their SOCs were high. Fig. 14 shows the variation in the power of the fuel cell system and the SOCs of both batteries, respectively. Table 7 summarizes the simulation results.

The operation time of pattern (b) is a little longer than that of pattern (a). That is because the power management strategy aimed to keep the SOC of battery as high as 50% by the remnant energy produced by the fuel cell system. It was also expected that the average load power of 334 W during the driving pattern (b) was smaller than the average load power of 395 W during the driving pattern (a), and less fuel was consumed for less frequent accelerations.

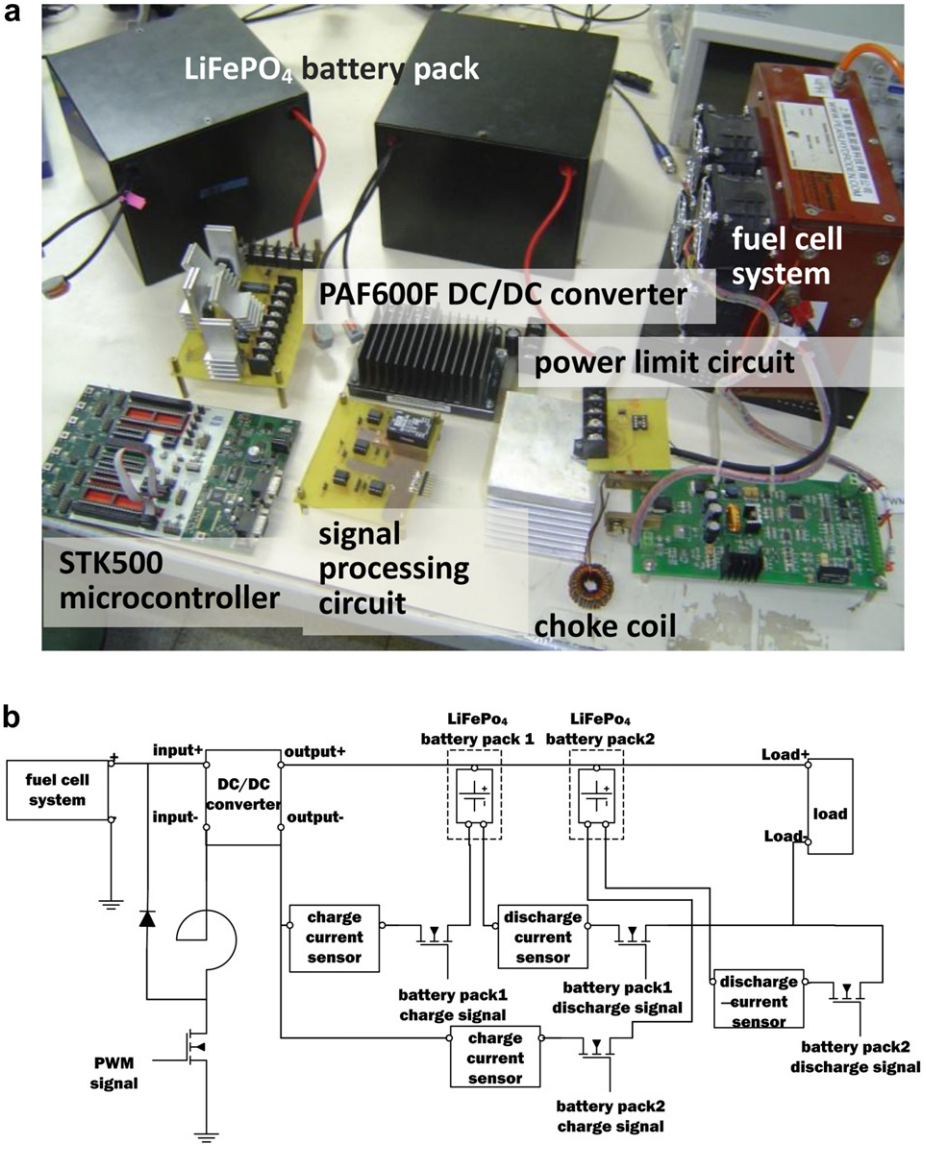

Fig. 15. Proposed hybrid fuel cell powertrain (a) experimental setup and (b) block diagram.

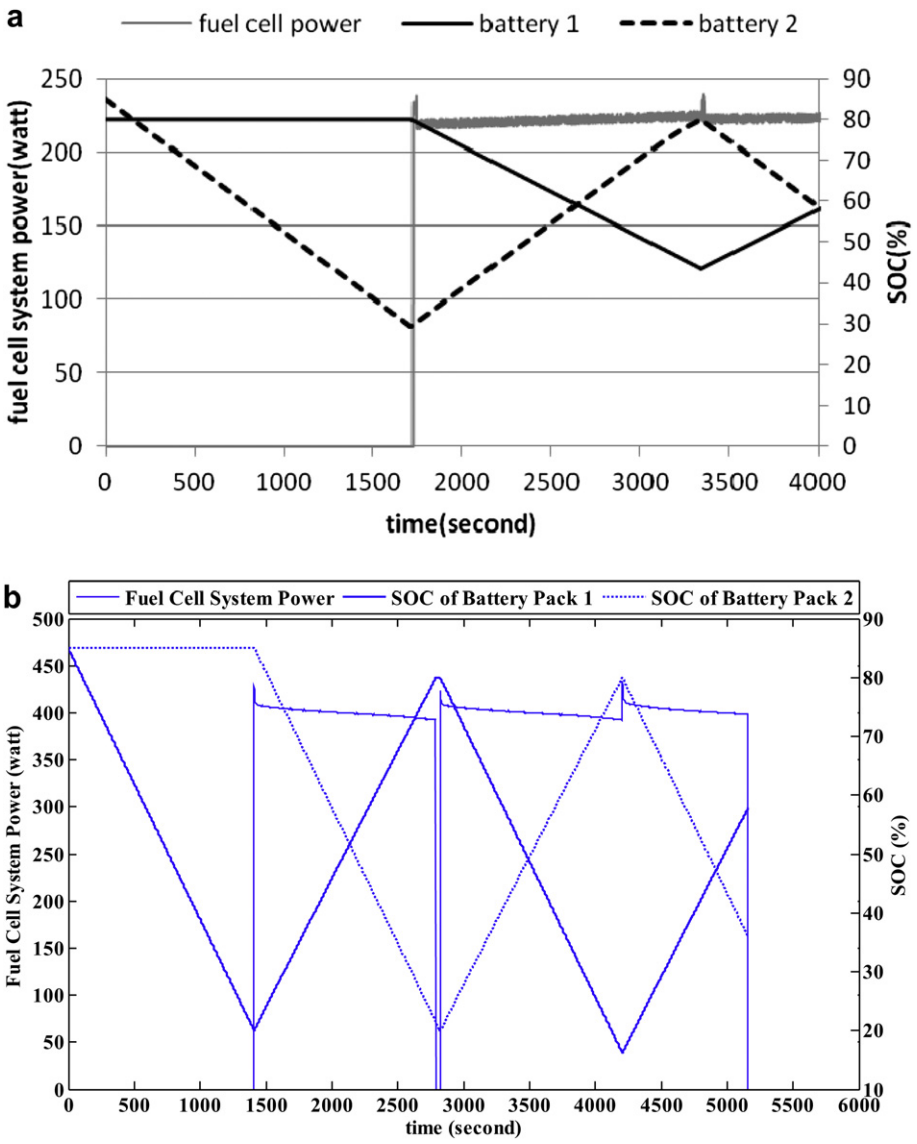

Fig. 16. Hybrid powertrain (a) experimental and (b) simulation results for the battery packs with high initial capacity.

4.4. Experiential validation

The test bench and its block diagram are presented in Fig. 15. The fuel cell system is supplied by a high-purity hydrogen tank on the anode side, while air is drawn by cooling fans on the cathode side. The fuel cell output voltage, ranging from 18 to 32 V, is adjusted to 28 V by a 600-W DC/DC converter PAF600F. A power limiter, which is composed of a 2.8-mH choke coil, an MOSFET of 100 V and 140 A, and a Shockley diode, is used to filter and regulate the fuel cell current before it flows to the DC/DC converter. Two battery packs, each with 8 serially connected $LiFePO_4$ battery cells, are connected with the load and DC/DC output. Four MOSFETs on the output side of the DC/DC converter are serially connected to the negative poles of the two battery packs, between which the "charge" and "discharge" states are switched. The state switching is managed by a microcontroller according to the estimated SOCs of battery packs and the operation scenarios prescribed in the previous section.

An electronic load is used to simulate a repetitive power consumption of the driving cycle of wheelchair. A 20-s duty simulates a constant-speed cruising period that consumes 140 W, while a consecutive 5-s duty simulates an acceleration mode that consumes 340 W. Before the experiment, the battery packs were first charged to a full SOC of 100%, and each of them was discharged at a constant current to a desired initial SOC. After resting for 2 hours, they were setup on the test bench for experiment. All the experiments were done on the room temperature between 20 and 25 °C. Three representative experiments where the total energy capacities of battery packs were initially different are presented and discussed as follows.

4.4.1. High initial capacity

Since both batteries had high initial SOCs over 80%, State DI was identified, as shown in Fig. 16. In the first 1700 s, battery 2 of higher SOC started to supply power to the load, while battery 1 stayed in the idled state. The fuel cell started to charge battery 2 when its SOC dropped to 30%, and battery 1 started to supply power to the load instead. The powertrain entered State DC around 1700 s. Around 3350 s, battery 2 took the discharge task

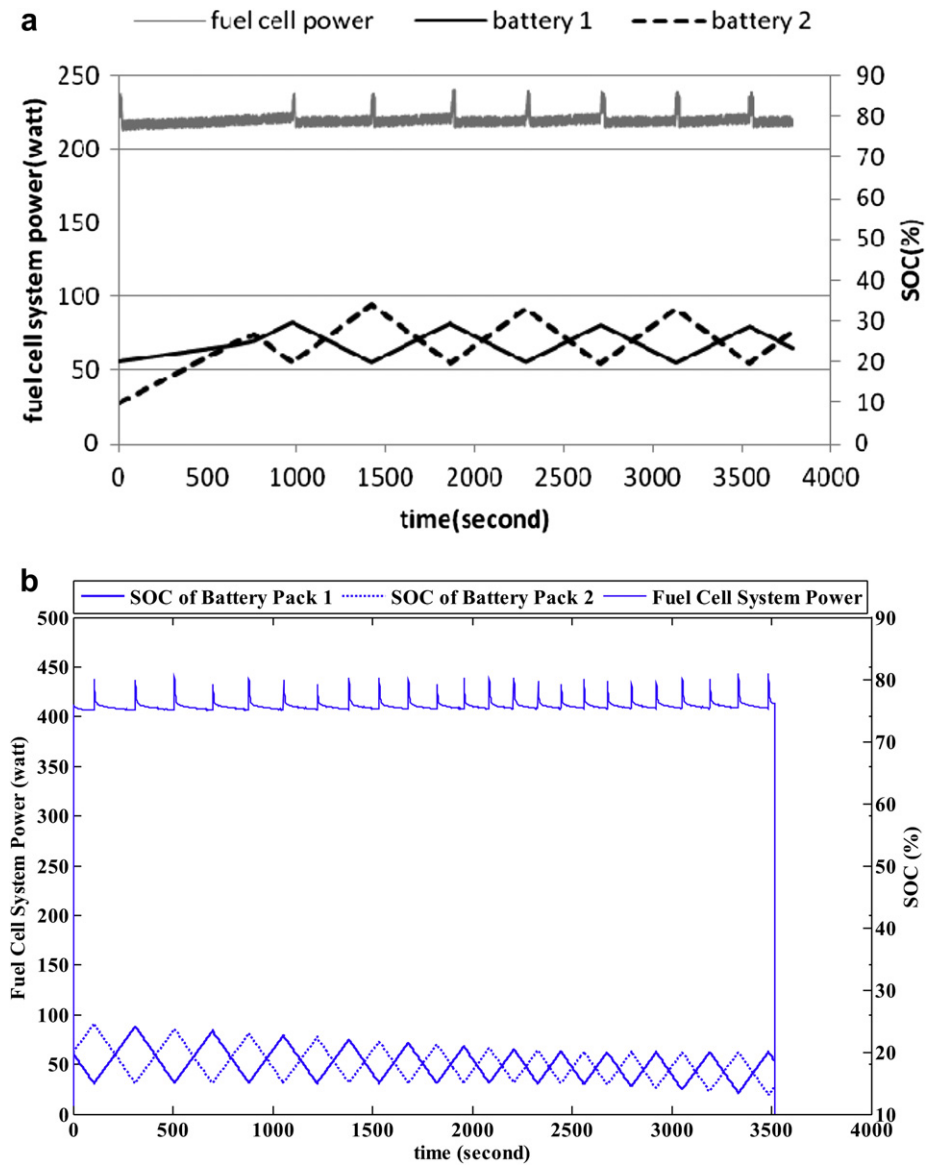

Fig. 17. Hybrid powertrain (a) experimental and (b) simulation results for the battery packs with low initial capacity.

after it was charged to have 80% SOC, while battery 1 was charged again even though its SOC was over 40%. Here, the powertrain maintained State DC.

Due to repetitive operation and aging, the fuel cell system and battery performance had been declining. The net output power of the fuel cell system in use would be limited under 230 W for safety. The current capacity of the two battery packs had also reduced so that only 8.86 A h and 5.76 A h were measured, respectively, during the discharging test at a constant current of 7 A.

4.4.2. Low initial capacity

This is the worst case when both battery packs had very low SOC below 20%, as shown in Fig. 17. They were not allowed to supply power to the load, but both stayed in the charge state, State CC. Until the SOC of battery 2 became 25% around 750 s and started to supply power to the load, while battery 1 was still charged by the fuel cell. The battery management policy would not allow any battery to drain its power lower than 20%. Therefore, when the SOC of battery 2 dropped to 20%, it was switched to be charged by the fuel cell, while battery 1, which was charged to a SOC about 35%, took the job to supply power to the load. The powertrain stayed in State DC continuously, but the charge and discharge states shifted between the two batteries.

It should be noted that the SOC of either battery may not be recharged to a higher SOC at the end of operation. It is suggested both SOCs of battery be charged at least as high as 40–50% before the standard operation.

4.4.3. Moderate initial capacity

The total residual capacity of batteries was initially in a safe state; one battery SOC at 80% and the other at 15%, as shown in Fig. 18. Therefore, the powertrain was initially identified as State DC. Battery 2 with higher SOC started to supply power to the load, while battery 1 with lower SOC was charged by the fuel cell. Over the whole period of experiment of 4000 s, operation states only shifted twice. Both batteries were successfully protected without

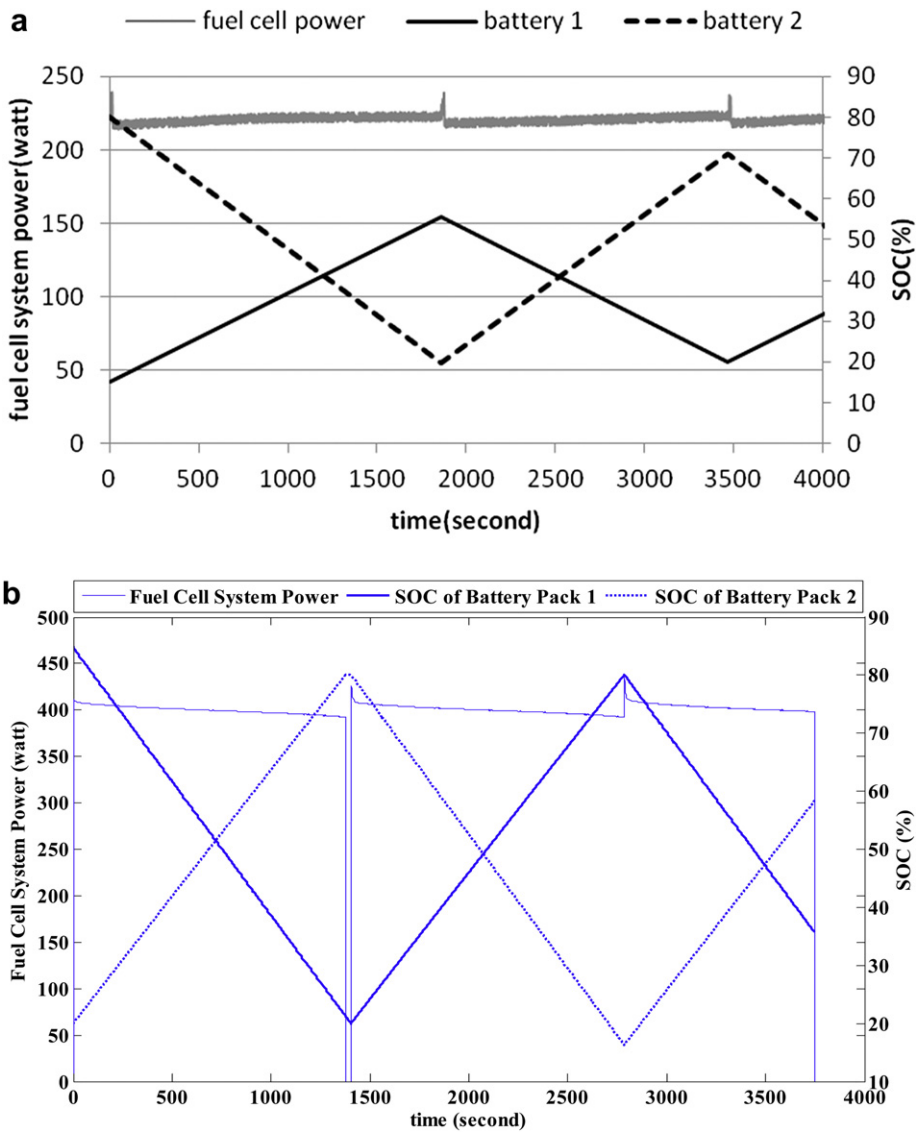

Fig. 18. Hybrid powertrain (a) experimental and (b) simulation results for the battery packs with moderate initial capacity.

frequent shifts between charge and discharge, and the fuel cell that worked at a steady state of power supply was also protected in a safe operation mode.

5. Conclusions

A novel hybrid fuel cell powertrain has been proposed for a powered wheelchair driven by rim motors. This powertrain consists of a fuel cell, a dc/dc converter, and two secondary battery packs, and its energy management strategy was made to solve the problems of frequent charging of secondary batteries and large power fluctuations of the fuel cell system. The hybrid fuel cell power system was simulated, and the simulation results showed that not only was the fuel cell able to operate efficiently near a constant power, but also the charging frequency of secondary batteries was reduced by about 98% compared to a series-hybrid fuel cell powertrain. Therefore, the durability and life cycle of the fuel cell and lithium iron phosphate battery packs may be improved. The proposed hybrid fuel cell powertrain has been successfully realized on a test bench to simulate the driving cycle of wheelchair, and it will be implemented on a novel powered wheelchair driven by rim motors.

Acknowledgment

This work was supported by the National Science Council of Taiwan, Republic of China, under Contract NSC97-2221-E-002-171-MY3 and NSC98-2622-B-002-008-CC2.

References

[1] P. Corbo, F. Migliardini, O. Veneri, J. Power Sources 195 (2010) 7849–7854.
[2] J. Bauman, M. Kazerani, IEEE Trans. Veh. Technol. 57 (2008) 760–769.
[3] M. Ouyang, L. Xu, J. Li, L. Lu, D. Gao, Q. Xie, J. Power Sources 163 (2006) 467–479.
[4] J. Wang, Y. Chen, Q. Chen, J. Power Sources 159 (2006) 1205–1213.
[5] G. Guizzi, M. Manno, M. de Falco, Int. J. Hydrogen Energy 34 (2009) 3112–3124.
[6] W. Greenwell, A. Vahidi, IEEE Trans. Ind. Electron. 57 (2010) 1954–1963.
[7] J. Larminie, A. Dicks, Fuel Cell Systems Explained, second ed. J. Wiley, Chichester, West Sussex, 2003.
[8] K. Çağatay Bayindir, M.A. Gözüküçük, A. Teke, Energy Convers. Manage. 52 (2011) 1305–1313.
[9] M. Van Wieringen, R. Pop-Iliev, IEEE Trans. Ind. Electron. 57 (2010) 641–648.

[10] A. Dalvi, M. Guay, Control Eng. Pract. 17 (2009) 924–938.
[11] J. Ryu, Y. Park, M. Sunwoo, J. Power Sources 195 (2010) 5735–5748.
[12] J. Bernard, S. Delprat, T.M. Guerra, F.N. Büchi, Control Eng. Pract. 18 (2010) 408–417.
[13] Y. Eren, O. Erdinc, H. Gorgun, M. Uzunoglu, B. Vural, Int. J. Hydrogen Energy 34 (2009) 8681–8694.
[14] C.Y. Li, G.P. Liu, J. Power Sources 192 (2009) 525–533.
[15] M.J. Kim, H. Peng, J. Power Sources 165 (2007) 819–832.
[16] K. Jeong, W. Lee, C. Kim, J. Power Sources 145 (2005) 319–326.
[17] V. Paladini, T. Donateo, A. de Risi, D. Laforgia, J. Fuel Cell Sci. Technol. 5 (2008) 021004.1–021004.8.
[18] L. Xu, J. Li, J. Hua, X. Li, M. Ouyang, J. Power Sources 194 (2009) 360–368.
[19] X. Li, L. Xu, J. Hua, X. Lin, J. Li, M. Ouyang, J. Power Sources 191 (2009) 542–549.
[20] P. Bubna, D. Brunner, S.G. Advani, A.K. Prasad, J. Power Sources 195 (2010) 6699–6708.
[21] X. Zhang, C.C. Mi, A. Masrur, D. Daniszewski, J. Power Sources 185 (2008) 1533–1543.
[22] G. Pede, A. Iacobazzi, S. Passerini, A. Bobbio, G. Botto, J. Power Sources 125 (2004) 280–291.
[23] P. Corbo, F. Corcione, F. Migliardini, O. Veneri, Energy Convers. Manage. 47 (2006) 3255–3271.
[24] P. Corbo, F. Migliardini, O. Veneri, J. Power Sources 181 (2008) 363–370.
[25] D. Gao, Z. Jin, Q. Lu, J. Power Sources 185 (2008) 311–317.
[26] O. Erdinc, B. Vural, M. Uzunoglu, J. Power Sources 194 (2009) 369–380.
[27] O. Erdinc, B. Vural, M. Uzunoglu, Y. Ates, Int. J. Hydrogen Energy 34 (2009) 5223–5233.
[28] A. Arce, A.J. del Real, C. Bordons, J. Process Control 19 (2009) 1289–1304.
[29] L. Xu, J. Li, J. Hua, X. Li, M. Ouyang, Int. J. Hydrogen Energy 34 (2009) 7323–7333.
[30] L.M. Fernandez, P. Garcia, C.A. Garcia, J.P. Torreglosa, F. Jurado, Int. J. Hydrogen Energy 35 (2010) 5731–5744.
[31] P. Bubna, D. Brunner, J.J. Gangloff Jr., S.G. Advani, A.K. Prasad, J. Power Sources 195 (2010) 3939–3949.
[32] P. Corbo, F. Migliardini, O. Veneri, Int. J. Hydrogen Energy 34 (2009) 4635–4644.
[33] X. Li, J. Li, L. Xu, F. Yang, J. Hua, M. Ouyang, Int. J. Hydrogen Energy 35 (2010) 3841–3847.
[34] J. Cao, A. Emadi, IEEE Trans. Power Electron. 27 (1) (2012) 941–946.
[35] Y.P. Yang, W.C. Huang, C.W. Lai, IET Electr. Power Appl. 1 (5) (2007) 825–832.
[36] Z. Liu, L. Yang, Z. Mao, W. Zhuge, Y. Zhang, L. Wang, J. Power Sources 157 (2006) 166–176.
[37] PSI International Semiconductor Co. Website: http://www.psi.com.tw/.
[38] M. Ehsani, Modern Electric, Hybrid Electric, and Fuel Cell Vehicles: Fundamentals, Theory, and Design, CRC Press, Boca Raton, 2005.
[39] Matlab Website: http://www.mathworks.com/matlabcentral.
[40] R.E. Sonnntag, C. Borgnakke, G.J. Van Wylen, Fundamentals of Thermodynamics, second ed. J. Wiley, Chichester, West Sussex, 2003.
[41] O. Tremblay, L. Dessaint, A. Dekkiche, A generic battery model for the dynamic simulation of hybrid electric vehicles, in: IEEE Vehicle Power and Propulsion Conference, Arlington, TX (2007) pp. 284–289.